Magneto-Optical Detection of the Spin Hall Effect in Pt and W Thin Films

C. Stamm,[1] C. Murer,[1] M. Berritta,[2] J. Feng,[1] M. Gabureac,[1] P. M. Oppeneer,[2] and P. Gambardella[1]
[1]Department of Materials, ETH Zürich, 8093 Zürich, Switzerland
[2]Department of Physics and Astronomy, Uppsala University, P.O. Box 516, SE-75120 Uppsala, Sweden
(Received 11 April 2017; published 25 August 2017)

The conversion of charge currents into spin currents in nonmagnetic conductors is a hallmark manifestation of spin-orbit coupling that has important implications for spintronic devices. Here we report the measurement of the interfacial spin accumulation induced by the spin Hall effect in Pt and W thin films using magneto-optical Kerr microscopy. We show that the Kerr rotation has opposite sign in Pt and W and scales linearly with current density. By comparing the experimental results with *ab initio* calculations of the spin Hall and magneto-optical Kerr effects, we quantitatively determine the current-induced spin accumulation at the Pt interface as 5×10^{-12} μ_B A^{-1} cm^2 per atom. From thickness-dependent measurements, we determine the spin diffusion length in a single Pt film to be 11 ± 3 nm, which is significantly larger compared to that of Pt adjacent to a magnetic layer.

DOI: 10.1103/PhysRevLett.119.087203

The spin Hall effect (SHE) converts an electric charge current flowing along a wire into a transverse spin current [1–3], leading to the accumulation of spins at the surface of the wire [4]. In nonmagnetic metals (NMs), the induced spin polarization is usually detected indirectly through its interaction with an adjacent ferromagnet (FM). Experimental methods to measure the SHE rely on the nonlocal resistance in lateral spin valve devices, in which the NM is either in contact [5] or separated from the FM electrodes [6], as well as on the spin pumping effect [7], the spin Hall magnetoresistance [8,9], and the detection of the SHE-induced spin-orbit torques [10–13] and magnetization reversal [14,15] in NM|FM bilayers. In such systems, however, magnetization-dependent scattering, interfacial spin-orbit coupling, and proximity effects deeply influence the spin accumulation [16], complicating the determination of the intrinsic SHE in the NM. Consequently, estimates of the charge-to-spin conversion ratio, namely the spin Hall angle θ_{SH}, and of the spin diffusion length l_s vary by more than 1 order of magnitude for the same metal [3]. In order to gain fundamental insight into the mechanisms leading to spin accumulation and optimize the spintronic devices that utilize the SHE, it is therefore essential to study the SHE directly in the NM layers.

A straightforward method to detect the SHE is to measure the resulting spin accumulation through the magneto-optical Kerr effect (MOKE). This technique has been employed to reveal the SHE in semiconductors, where l_s is of the order of a few μm and the spin accumulation can be laterally resolved by polarization-sensitive MOKE microscopy [17,18]. The situation is much more difficult in the case of a metallic conductor such as Pt, where l_s is just a few nm. Not only is it unfeasible to detect the lateral spin accumulation with optical wavelengths, but the magnitude of the spin accumulation scales with l_s and is, despite the relatively large θ_{SH}, 1 to 2 orders of magnitude smaller compared to semiconductors. Nevertheless, preliminary experiments have been performed to directly study the spin accumulation in heavy-metal films by the MOKE. A report by van 't Erve *et al.* [19] claims a spin accumulation signal on an 8-nm-thick film of β-W and, although less clear, on a 20-nm-thick film of Pt. The apparent sign change of the observed effect is argued to prove that the polarization rotation, amounting to 3×10^{-4} rad for β-W, is due to the SHE. A follow-up study by Riego *et al.* [20], however, does not support the above conclusions. In that work, magneto-optic ellipsometry measurements with a Kerr rotation detection limit of 10^{-7} rad show that any observed current-induced effect is related to a change of the reflectivity of the sample caused by Joule heating. More recently, Su *et al.* [21] came to similar conclusions, arguing that MOKE detection would require a current density j larger than 10^8 $A\,cm^{-2}$. In fact, all three studies [19–21] used j in the order of 10^5 $A\,cm^{-2}$, which leads to an estimated Kerr rotation of the order of 10^{-9} rad [21], 5 orders of magnitude smaller than the rotation reported initially [19]. Alternative optical approaches to detect the spin accumulation in NMs include Brillouin light scattering [22] and second harmonic generation [23]. Using the latter technique, Pattabi *et al.* [23] reported evidence of current-induced spin accumulation in Pt, demonstrating also the feasibility of time-resolved studies. However, the interpretation of the second harmonic signal is not as straightforward as it is for the MOKE.

In this Letter, we demonstrate the unambiguous detection of the SHE in heavy metals using linear magneto-optical measurements combined with current modulation techniques. We use scanning MOKE microscopy with a sensitivity of 5×10^{-9} rad to detect the spin accumulation at the surfaces of Pt and W wires caused by the SHE. Additionally, we perform *ab initio* linear response calculations of the SHE and magneto-optical Kerr rotation [24] caused by the spin accumulation. Comparison of the experimental data with the *ab initio* MOKE calculations

provides quantitative values for the spin accumulation, the spin diffusion length, and the spin Hall angle of Pt. These measurements provide a reliable estimate of the SHE and spin diffusion parameters in a NM, without an adjacent FM.

Our samples are lithographically patterned Hall bars of Pt and W with line widths of 10 and 20 μm [Fig. 1(a)]. The Pt films, with thicknesses ranging between 5 and 60 nm, and 10-nm-thick W films are deposited by sputtering on oxidized Si substrates. Four-terminal measurements show that the resistivity of Pt varies between $\rho = 27$ and 16 $\mu\Omega\,$cm with increasing thickness, whereas the resistivity of W is $\rho = 164$ $\mu\Omega\,$cm, indicative of β-phase W. For the MOKE measurement, a laser beam with wavelength $\lambda =$ 514 nm is focused to $\approx$1 μm spot size onto the sample, which is mounted on a piezo scanner. A sine-modulated current with variable amplitude up to $j = 1.5 \times 10^7\,\mathrm{A\,cm^{-2}}$ runs through the central conductor, inducing edge spin accumulation [arrows in Fig. 1(b)]. The resulting light polarization rotation is measured using a sensitive detection scheme comprising a polarization-splitting Wollaston prism and a balanced photodetector. Half of the beam is sent onto a photodiode for measuring changes of the reflected intensity. Both signals are measured by lock-in amplifiers that record the fundamental frequency of the Kerr rotation amplitude and the second harmonic contribution of the reflected intensity. More details about the setup are given in Ref. [25].

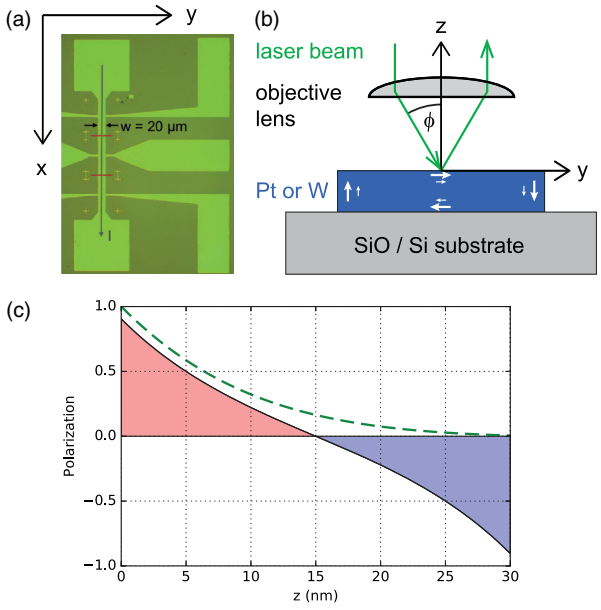

FIG. 1. (a) Microscope image of a Pt Hall bar with the current running top-down (parallel to x). (b) Laser beam path through the focusing objective. The arrows in the Pt or W wire represent the spin accumulation. (c) Depth profile of the calculated spin accumulation (shaded) in a 30-nm-thick wire for $l_s = 9$ nm. The dashed line represents the depth-dependent sensitivity of the MOKE.

In a longitudinal MOKE measurement we detect the accumulation of spins along the in-plane y direction transverse to the electric current flowing along x, as illustrated in Figs. 1(a) and 1(b). A consequence of the transverse spin current generated by the SHE is the accumulation of spins of opposite sign at opposite interfaces. We therefore detect the superposition of the polarization rotation from spins accumulated at the top and bottom interfaces, drawn as shaded areas in Fig. 1(c). For quantitative analysis one needs to take into account the light attenuation of the probing laser beam in the conductive material, drawn as a dashed line in Fig. 1(c), as modeled by depth-dependent MOKE calculations [39,40]. At the same time, the material-dependent l_s determines the spatial distribution and the amount of spin accumulation [4], which will be reduced for films of thickness t comparable or smaller than l_s. These effects will lead to a saturation of the spin accumulation detected by the MOKE for films of sufficient thickness. From a thickness-dependent study we can therefore extract the intrinsic spin accumulation and l_s of a single Pt film, as opposed to the usual Pt-FM bilayer.

We first describe the effect of current injection on the optical reflectivity of Pt and W, which is at the origin of controversial MOKE experiments [19–21]. Figure 2 displays the results from scanning the laser beam in the

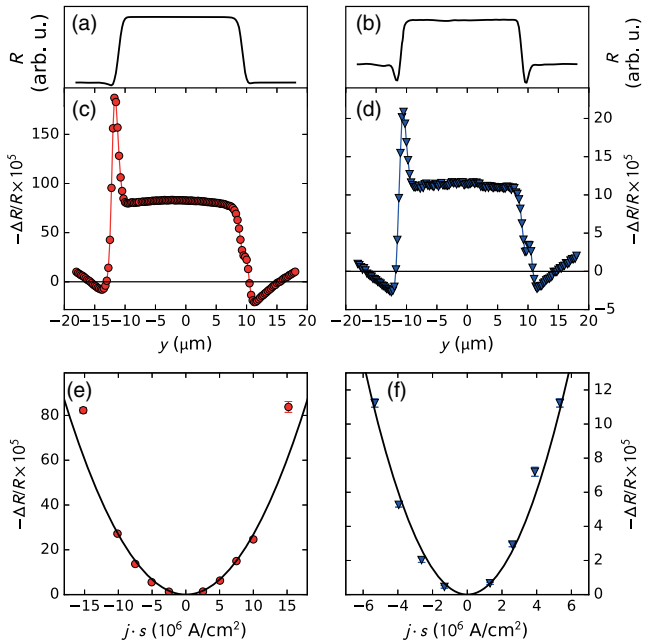

FIG. 2. (a), (b) Line scans of the optical reflectivity across 20-μm-wide wires of (a) 15-nm Pt and (b) 10-nm W. (c), (d) Thermally induced change of the reflectivity $-\Delta R/R$ for (c) Pt at $j = 1.5 \times 10^7\,\mathrm{A\,cm^{-2}}$ and (d) W at $j = 5.3 \times 10^6\,\mathrm{A\,cm^{-2}}$. (e), (f) Current dependence of $-\Delta R/R$ for (e) Pt and (f) W. The solid lines are fits to a j^2 function. Points left of the origin were measured with the reversed optical path, with s denoting the sign of the incidence angle of the laser beam.

y direction across the Hall bar while injecting a sinusoidal current. Both materials, Pt and W, exhibit a change of the reflected intensity R, plotted in Fig. 2. The relative change $\Delta R/R$, measured in the intensity photodiode as second harmonic of the sine current normalized by the average R, scales as j^2 and has the same sign in Pt and W. We therefore assign it to temperature-induced changes of the reflectivity [41] due to Joule heating. Using the relationship $\Delta R/R = c_{TR}\Delta T$, where $c_{TR} = -0.58 \times 10^{-4}$ K^{-1} for Pt [41], we estimate a temperature raise ΔT ranging from 0.2 to 14.3 K as j increases from 2.5×10^6 to 1.5×10^7 A cm^{-2}.

Crucial for our study is the Kerr rotation, which is measured as the voltage output of the balanced detector at the fundamental frequency of the driving current and calibrated using a half-wave plate. Figures 3(a) and 3(b) show the Kerr rotation angle θ_K measured on 15-nm-thick Pt and 10-nm-thick W during sinusoidal current injection. We observe a clear Kerr rotation signal from the surface of the conducting wires, which is of the order of a few tens of nrad and has opposite sign in Pt and W. Apart from spurious edge effects, which we attribute to irregular light reflections at the sample boundaries, θ_K is approximately constant over the wire surface, consistent with the spin accumulation picture in Fig. 1(b). Moreover, we find that θ_K varies linearly with the applied current, as shown in Figs. 3(c) and 3(d).

Further evidence that θ_K stems from the accumulated spins at both interfaces and is, thus, a direct consequence of the SHE in the heavy-metal layer comes from the following considerations. First, the sine modulation employed here

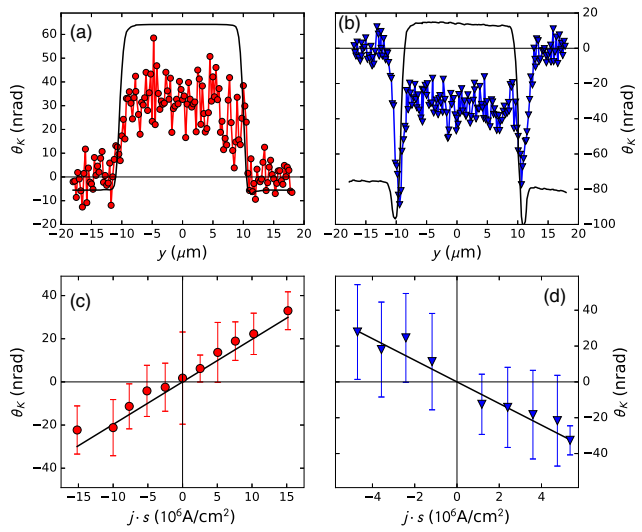

FIG. 3. SHE-induced Kerr rotation. (a) Line scan of θ_K across a 20-μm-wide, 15-nm-thick Pt wire at a current density $j = 1.5 \times 10^7$ A cm^{-2} and (b) a 10-nm-thick W wire at $j = 5.3 \times 10^6$ A cm^{-2}. (c), (d) θ_K as a function of j. The data points represent line scan averages; statistical error bars from averaging multiple line scans are indicated. The solid lines are linear fits to the data. Points left of the origin were measured with the reversed optical path, s.

allows for the harmonic separation of different signal contributions, notably the change of the optical reflectivity proportional to j^2 (Fig. 2) and the linear dependence of θ_K on j (Fig. 3). In contrast, current switching by square wave modulation, as employed in previous studies [19–21], cannot distinguish these effects. We verified that even a slight mismatch between the amplitude of positive and negative current pulses leads to large spurious thermal signals at the fundamental modulation frequency, as discussed also in Ref. [21]. Additionally, we implemented an automatic relay scheme that physically inverts the current flowing in the samples and allows us to average out any remaining thermal artifact [25]. Second, control measurements on an Al wire did not result in a detectable Kerr rotation [25], as expected for a light metal with a minute SHE and large l_s [5]. Third, in the longitudinal Kerr geometry chosen here, we are sensitive to spin signatures in the yz scattering plane, i.e., to the in-plane components along y and perpendicular ones along z. The two contributions exhibit odd and even symmetry upon inversion of the light incidence angle, for the y and z components, respectively. Figures 3(c) and (d) report θ_K measured with opposite angles of incidence in the two halves of each diagram, which prove that the Kerr rotation changes sign by reversing the optical path of the laser beam. The data are fitted by a line that, within error bars, intersects the origin. This demonstrates the absence of any thermally induced signal that could be introduced after the switching relay, and excludes the presence of a polar contribution, i.e., a magnetization along z. By rotating the sample by 90° about the surface normal, we also exclude a magnetization along x [25]. We therefore conclude that our signal results uniquely from the in-plane spin accumulation along y.

To relate the measured Kerr rotation to the amount of accumulated spins we performed *ab initio* calculations of the SHE and of the MOKE due to accumulated spins in Pt and W. We use the density-functional theory framework in the local spin-density approximation to compute the relativistic electronic structure, and employ the linear-response theory to calculate the spin- and frequency-dependent Hall conductivity $\sigma^y_{xz}(\omega)$ (with y indicating the spin quantization axis) [42] as well as the off-diagonal and diagonal optical conductivities, $\sigma_{ij}(\omega)$ [24]. The dc spin Hall conductivity is given by $\sigma^{\mathrm{SH}}_{xz} = \mathrm{Re}[\sigma^{\uparrow}_{xz}(\omega) - \sigma^{\downarrow}_{xz}(\omega)]/2$, for $\omega \to 0$. The calculated $\mathrm{Re}[\sigma^y_{xz}(\omega)]$ conductivities of fcc Pt and bcc α-W are shown in Figs. 4(a) and 4(b); more details are given in Ref. [25]. The spin-dependent Hall conductivities are antisymmetric in the spin projection and the dc spin Hall conductivities of Pt and W have opposite signs. To investigate the possibility of a feedback effect on the SHE due to the spin accumulation, we calculated the spin-dependent Hall conductivities in the presence of an induced magnetization [dashed curves in Figs. 4(a) and 4(b)] and find that its influence is negligible. The calculated spin Hall conductivity of Pt, $\sigma^{\mathrm{SH}}_{xz}(\mathrm{Pt}) = 1890\ \Omega^{-1}\,\mathrm{cm}^{-1}$, is

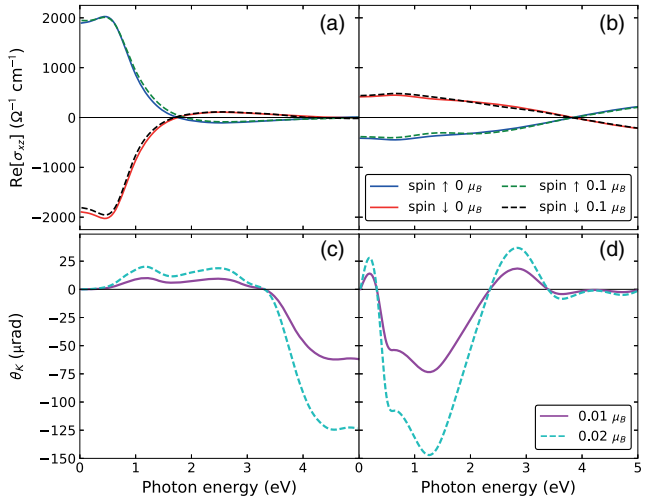

FIG. 4. *Ab initio* spin-resolved Hall conductivity $\mathrm{Re}[\sigma^y_{xz}(\omega)]$ as a function of photon energy $\hbar\omega$ of (a) Pt and (b) W. The influence of a spin accumulation on the calculated $\mathrm{Re}[\sigma^y_{xz}(\omega)]$ is shown by the dashed curves (for an induced magnetization of $M^y = 0.1\ \mu_B$ per atom). (c,d) Calculated longitudinal Kerr rotation spectrum for s-polarized light incident at 37° in the yz plane, for $M^y = 0.01\ \mu_B$ (magenta line) and $M^y = 0.02\ \mu_B$ (dashed cyan line) for Pt and W, respectively.

furthermore in agreement with previous calculations [43–45] and well within the range of measured values ($\sim 1900 \pm 500\ \Omega^{-1}\,\mathrm{cm}^{-1}$ [46]). Next, we compute the longitudinal Kerr rotation θ_K spectrum for s-polarized light as a function of the induced y magnetization (M^y) in Pt and W. The results are shown in Figs. 4(c) and 4(d), where, for better visibility, we show the curves corresponding to $M^y = 0.01\mu_B$ and $0.02\mu_B$ per atom, having verified that θ_K scales linearly with M^y. This information will be used in the following, where we limit the discussion to Pt, for which there is no ambiguity of crystal structure.

We use the *ab initio* calculated $\sigma^{\mathrm{SH}}_{xz}$ and MOKE per μ_B to compute the spin accumulation in Pt, then compute the theoretical θ_K, and compare it with our experiment. By solving the drift-diffusion equation for spins polarized parallel to y and $-y$ for a film of thickness t [4], we obtain the spin accumulation potential

$$V^y_s(z) = 4 l_s \sigma^{\mathrm{SH}}_{xz} \rho^2 j \sinh\left(\frac{t-2z}{2l_s}\right)\left[\cosh\left(\frac{t}{2l_s}\right)\right]^{-1}. \quad (1)$$

The induced magnetization profile (in μ_B) can then be calculated as $M^y(z) = \frac{1}{2} e V^y_s(z) D(E_{\mathrm{F}}) F$, where e is the electron's charge, $D(E_{\mathrm{F}}) = 1.67$ states/eV is the *ab initio* calculated density of states at the Fermi energy, and $F = 2$ is the Stoner enhancement factor of Pt [47]. Using the depth sensitivity of longitudinal MOKE [39], we derive the Kerr rotation expected in a measurement of a thin film [25],

$$\theta_K = \frac{l_s \sigma^{\mathrm{SH}}_{xz} \rho^2 j D(E_{\mathrm{F}}) F e^{t/2l_s}}{\cosh(t/2l_s)} \times \mathrm{Re}\left\{\Phi^{\mathrm{bulk}}_K \kappa \left(\frac{(e^{-\kappa^- t}-1)e^{-t/l_s}}{\kappa^-} - \frac{e^{-\kappa^+ t}-1}{\kappa^+}\right)\right\}, \quad (2)$$

where Φ^{bulk}_K is the bulk complex Kerr effect, and we have defined $\kappa = (4\pi i \bar{n}\cos\psi)/\lambda$, $\cos\psi = (1 - \sin^2\phi_i/\bar{n}^2)^{1/2}$, with $\bar{n}$ the complex index of refraction, ϕ_i the angle of incidence, and $\kappa^{\pm} = \kappa \pm 1/l_s$. From our *ab initio* calculations we obtain values for $\sigma^{\mathrm{SH}}_{xz}$, $\bar{n}$, and Φ^{bulk}_K [25], while other quantities are given from the experiment (ρ, t, j, ϕ_i).

Figure 5 compares the experimental and computed θ_K of Pt as a function of film thickness for a current density $j = 10^7\ \mathrm{A\,cm}^{-2}$. We observe that, after an initial increase, θ_K saturates for $t \gtrsim 30$ nm. This behavior can be understood when one considers two effects, the limited probing depth of our optical measurements and the opposite spin accumulation at the top and bottom interfaces due to the SHE. The solid line represents a fit of θ_K computed using Eq. (2) taking the average resistivity $\rho = 20.6\ \mu\Omega\,\mathrm{cm}$ from the experiment and $\sigma^{\mathrm{SH}}_{xz}$ and l_s as free parameters. The fit gives $\sigma^{\mathrm{SH}}_{xz} = 1880\ \Omega^{-1}\,\mathrm{cm}^{-1}$, in excellent agreement with theory, and $l_s = 11.4$ nm. These values represent, to our knowledge, the first estimate of the intrinsic l_s and $\sigma^{\mathrm{SH}}_{xz}$ of Pt, independently from the proximity with other metals. The spin Hall angle obtained from this fit is $\theta_{\mathrm{SH}} = 2\sigma^{\mathrm{SH}}_{xz}\rho = 0.08 \pm 0.02$, where the error accounts for the thickness dependence of ρ [25]. Our l_s is significantly larger than that reported for NM|FM bilayers ($l_s \approx 1$–2 nm [3]), and closer to that obtained by measuring spin absorption in nonlocal devices ($l_s = 2$–11 nm, depending on ρ and temperature [46,48]). We note that our estimate assumes constant $\sigma^{\mathrm{SH}}_{xz}$, ρ, and l_s parameters, consistently with the derivation of Eq. (1). However, if

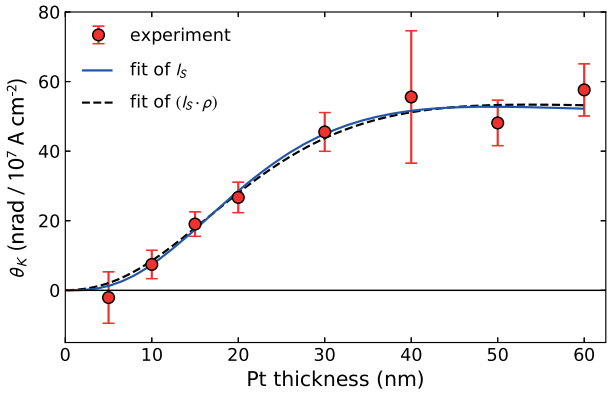

FIG. 5. Kerr rotation vs Pt thickness for $j = 10^7\ \mathrm{A\,cm}^{-2}$. The symbols are obtained from linear fits of θ_K as a function of j, as shown in Fig. 3. The solid curve is a fit using Eq. (2) and $\sigma^{\mathrm{SH}}_{xz} = 1880\ \Omega^{-1}\,\mathrm{cm}^{-1}$, $l_s = 11.4$ nm as free parameters. The dashed line is a fit with constant $l_s\rho = 2.6\ \mathrm{f\Omega m}^2$.

Elliott-Yafet spin relaxation dominates in Pt, one expects $l_s \propto \rho^{-1}$ [46,49,50]. If we take this constraint into account, together with the experimental variation of ρ, our fit gives $\sigma_{xz}^{\mathrm{SH}} = 1790\ \Omega^{-1}\ \mathrm{cm}^{-1}$ and $l_s\rho = 2.6\,\mathrm{f\Omega m}^2$ [dashed line in Fig. (5)]. The latter value is larger than $l_s\rho = 0.6 - 1.3\,\mathrm{f\Omega m}^2$ reported by other techniques [46,48–51], as discussed in Ref. [25].

Finally, by using the proportionality constant between θ_K and the induced magnetic moment [25], we estimate that the magnetization detected by the MOKE at a current density $j = 10^7\ \mathrm{A\,cm}^{-2}$ in the thicker Pt films ($t \geq 40$ nm) corresponds to $(5.0 \pm 0.6) \times 10^{-5}\ \mu_B/\mathrm{atom}$ in the topmost layer, whereas the average magnetization in the upper half of the films is $(2.0 \pm 0.2) \times 10^{-5}\ \mu_B/\mathrm{atom}$.

In conclusion, we have used MOKE microscopy combined with *ab initio* calculations of MOKE and spin Hall conductivity to measure the spin accumulation caused by the SHE in Pt and W thin films. Our results demonstrate the feasibility of characterizing the SHE in NM using magneto-optical methods, independently of the presence of another metal, opening the way to map the spatial and temporal evolution of the spin accumulation and diffusive dynamics in materials with strong spin-orbit coupling and small l_s.

We acknowledge funding by the Swiss National Science Foundation (Grants No. 200021-153404 and No. 200020-172775), the Swedish Research Council (VR), the K. and A. Wallenberg Foundation (Grant No. 2015.0060), and the Swedish National Infrastructure for Computing (SNIC).

[1] M. I. Dyakonov and V. I. Perel, Pis'ma Zh. Eksp. Teor. Fiz. **13**, 657 (1971).
[2] J. E. Hirsch, Phys. Rev. Lett. **83**, 1834 (1999).
[3] J. Sinova, S. O. Valenzuela, J. Wunderlich, C. H. Back, and T. Jungwirth, Rev. Mod. Phys. **87**, 1213 (2015).
[4] S. Zhang, Phys. Rev. Lett. **85**, 393 (2000).
[5] S. O. Valenzuela and M. Tinkham, Nature (London) **442**, 176 (2006).
[6] Y. Niimi and Y. Otani, Rep. Prog. Phys. **78**, 124501 (2015).
[7] E. Saitoh, M. Ueda, H. Miyajima, and G. Tatara, Appl. Phys. Lett. **88**, 182509 (2006).
[8] H. Nakayama, M. Althammer, Y.-T. Chen, K. Uchida, Y. Kajiwara, D. Kikuchi, T. Ohtani, S. Geprägs, M. Opel, S. Takahashi, R. Gross, G. E. W. Bauer, S. T. B. Goennenwein, and E. Saitoh, Phys. Rev. Lett. **110**, 206601 (2013).
[9] C. O. Avci, K. Garello, A. Ghosh, M. Gabureac, S. F. Alvarado, and P. Gambardella, Nat. Phys. **11**, 570 (2015).
[10] K. Ando, S. Takahashi, K. Harii, K. Sasage, J. Ieda, S. Maekawa, and E. Saitoh, Phys. Rev. Lett. **101**, 036601 (2008).
[11] L. Liu, T. Moriyama, D. C. Ralph, and R. A. Buhrman, Phys. Rev. Lett. **106**, 036601 (2011).
[12] K. Garello, I. M. Miron, C. O. Avci, F. Freimuth, Y. Mokrousov, S. Blugel, S. Auffret, O. Boulle, G. Gaudin, and P. Gambardella, Nat. Nanotechnol. **8**, 587 (2013).
[13] X. Fan, H. Celik, J. Wu, C. Ni, K.-J. Lee, V. O. Lorenz, and J. Q. Xiao, Nat. Commun. **5**, 3042 (2014).
[14] I. M. Miron, K. Garello, G. Gaudin, P.-J. Zermatten, M. V. Costache, S. Auffret, S. Bandiera, B. Rodmacq, A. Schuhl, and P. Gambardella, Nature (London) **476**, 189 (2011).
[15] L. Liu, C.-F. Pai, Y. Li, H. W. Tseng, D. C. Ralph, and R. A. Buhrman, Science **336**, 555 (2012).
[16] V. P. Amin and M. D. Stiles, Phys. Rev. B **94**, 104420 (2016).
[17] Y. K. Kato, R. C. Myers, A. C. Gossard, and D. D. Awschalom, Science **306**, 1910 (2004).
[18] V. Sih, R. C. Myers, Y. K. Kato, W. H. Lau, A. C. Gossard, and D. D. Awschalom, Nat. Phys. **1**, 31 (2005).
[19] O. M. J. van 't Erve, A. T. Hanbicki, K. M. McCreary, C. H. Li, and B. T. Jonker, Appl. Phys. Lett. **104**, 172402 (2014).
[20] P. Riego, S. Vélez, J. M. Gomez-Perez, J. A. Arregi, L. E. Hueso, F. Casanova, and A. Berger, Appl. Phys. Lett. **109**, 172402 (2016).
[21] Y. Su, H. Wang, J. Li, C. Tian, R. Wu, X. Jin, and Y. R. Shen, Appl. Phys. Lett. **110**, 042401 (2017).
[22] F. Fohr, S. Kaltenborn, J. Hamrle, H. Schultheiß, A. A. Serga, H. C. Schneider, B. Hillebrands, Y. Fukuma, L. Wang, and Y. Otani, Phys. Rev. Lett. **106**, 226601 (2011).
[23] A. Pattabi, Z. Gu, J. Gorchon, Y. Yang, J. Finley, O. J. Lee, H. A. Raziq, S. Salahuddin, and J. Bokor, Appl. Phys. Lett. **107**, 152404 (2015).
[24] P. M. Oppeneer, in *Handbook of Magnetic Materials*, Vol. 13, edited by K. H. J. Buschow (Elsevier, Amsterdam, 2001), Chap. 3, pp. 229–422.
[25] See Supplemental Material at http://link.aps.org/supplemental/10.1103/PhysRevLett.119.087203, which includes Refs. [26–38], for a detailed description of the experimental setup, theory, additional measurements of the SHE in Pt and Al, and a discussion of the fits of l_s.
[26] C.-F. Pai, L. Liu, Y. Li, H. W. Tseng, D. C. Ralph, and R. A. Buhrman, Appl. Phys. Lett. **101**, 122404 (2012).
[27] Q. Hao, W. Chen, and G. Xiao, Appl. Phys. Lett. **106**, 182403 (2015).
[28] A. R. Williams, J. Kübler, and C. D. Gelatt, Phys. Rev. B **19**, 6094 (1979).
[29] V. Eyert, *The Augmented Spherical Wave Method* (Springer, Heidelberg, 2007).
[30] U. von Barth and L. Hedin, J. Phys. C **5**, 1629 (1972).
[31] P. M. Oppeneer, T. Maurer, J. Sticht, and J. Kübler, Phys. Rev. B **45**, 10924 (1992).
[32] R. Mondal, M. Berritta, K. Carva, and P. M. Oppeneer, Phys. Rev. B **91**, 174415 (2015).
[33] W. Zhang, M. B. Jungfleisch, W. Jiang, Y. Liu, J. E. Pearson, S. G. te Velthuis, A. Hoffmann, F. Freimuth, and Y. Mokrousov, Phys. Rev. B **91**, 115316 (2015).
[34] C.-Y. You and S.-C. Shin, Appl. Phys. Lett. **69**, 1315 (1996).
[35] M. A. Ordal, R. J. Bell, R. W. Alexander, L. L. Long, and M. R. Querry, Appl. Opt. **24**, 4493 (1985).
[36] Y.-T. Chen, S. Takahashi, H. Nakayama, M. Althammer, S. T. B. Goennenwein, E. Saitoh, and G. E. W. Bauer, Phys. Rev. B **87**, 144411 (2013).
[37] J. Ryu, M. Kohda, and J. Nitta, Phys. Rev. Lett. **116**, 256802 (2016).
[38] F. Freimuth, S. Blügel, and Y. Mokrousov, Phys. Rev. B **92**, 064415 (2015).

[39] G. Traeger, L. Wenzel, and A. Hubert, Phys. Status Solidi (a) **131**, 201 (1992).
[40] J. Hamrle, J. Ferré, M. Nývlt, and Š. Višňovský, Phys. Rev. B **66**, 224423 (2002).
[41] T. Favaloro, J.-H. Bahk, and A. Shakouri, Rev. Sci. Instrum. **86**, 024903 (2015).
[42] P. M. Oppeneer and A. Liebsch, J. Phys. Condens. Matter **16**, 5519 (2004).
[43] G. Y. Guo, S. Murakami, T.-W. Chen, and N. Nagaosa, Phys. Rev. Lett. **100**, 096401 (2008).
[44] T. Tanaka, H. Kontani, M. Naito, T. Naito, D. S. Hirashima, K. Yamada, and J. Inoue, Phys. Rev. B **77**, 165117 (2008).
[45] L. Wang, R. J. H. Wesselink, Y. Liu, Z. Yuan, K. Xia, and P. J. Kelly, Phys. Rev. Lett. **116**, 196602 (2016).
[46] E. Sagasta, Y. Omori, M. Isasa, M. Gradhand, L. E. Hueso, Y. Niimi, Y. C. Otani, and F. Casanova, Phys. Rev. B **94**, 060412 (2016).
[47] O. Gunnarsson, J. Phys. F **6**, 587 (1976).
[48] Y. Niimi, D. Wei, H. Idzuchi, T. Wakamura, T. Kato, and Y. C. Otani, Phys. Rev. Lett. **110**, 016805 (2013).
[49] J.-C. Rojas-Sánchez, N. Reyren, P. Laczkowski, W. Savero, J.-P. Attané, C. Deranlot, M. Jamet, J.-M. George, L. Vila, and H. Jaffrès, Phys. Rev. Lett. **112**, 106602 (2014).
[50] M.-H. Nguyen, D. C. Ralph, and R. A. Buhrman, Phys. Rev. Lett. **116**, 126601 (2016).
[51] Y. Liu, Z. Yuan, R. J. H. Wesselink, A. A. Starikov, and P. J. Kelly, Phys. Rev. Lett. **113**, 207202 (2014).